Orion Optical Navigation Progress Toward Exploration Mission 1

Greg N. Holt*, Christopher N. D'Souza†, and David Saley‡
NASA Johnson Space Center, 2101 NASA Parkway, Houston, TX, 77058

Optical navigation of human spacecraft was proposed on Gemini and implemented successfully on Apollo as a means of autonomously operating the vehicle in the event of lost communication with controllers on Earth. The Orion emergency return system utilizing optical navigation has matured in design over the last several years, and is currently undergoing the final implementation and test phase in preparation for Exploration Mission 1 (EM-1) in 2019. The software development is past its Critical Design Review, and is progressing through test and certification for human rating. The filter architecture uses a square-root-free UDU covariance factorization. Linear Covariance Analysis (LinCov) was used to analyze the measurement models and the measurement error models on a representative EM-1 trajectory. The Orion EM-1 flight camera was calibrated at the Johnson Space Center (JSC) electro-optics lab. To permanently stake the focal length of the camera a 500 mm focal length refractive collimator was used. Two Engineering Design Unit (EDU) cameras and an EDU star tracker were used for a live-sky test in Denver. In-space imagery with high-fidelity truth metadata is rare so these live-sky tests provide one of the closest real-world analogs to operational use. A hardware-in-the-loop test rig was developed in the Johnson Space Center Electro-Optics Lab to exercise the OpNav system prior to integrated testing on the Orion vehicle. The software is verified with synthetic images. Several hundred off-nominal images are also used to analyze robustness and fault detection in the software. These include effects such as stray light, excess radiation damage, and specular reflections, and are used to help verify the tuning parameters chosen for the algorithms such as earth atmosphere bias, minimum pixel intensity, and star detection thresholds.

I. Background

Optical navigation of human spacecraft was proposed on Gemini and implemented successfully on Apollo as a means of autonomously operating the vehicle in the event of lost communication with controllers on Earth. This application was quintessentially summarized in the epilogue to Battin.[1] It shares a history with the "method of lunar distances" that was used in the 18th century and gained some notoriety after its use by Captain James Cook during his 1768 Pacific voyage of the *HMS Endeavor*. The Orion emergency return system utilizing optical navigation has matured in design over the last several years, and is currently undergoing the final implementation and test phase in preparation for Exploration Mission 1 (EM-1) in 2019. The software development is being worked as a Government Furnished Equipment (GFE) project delivered as an application within the Core Flight Software of the Orion camera controller module.

A. Concept of Operations

The Orion optical navigation system uses a body fixed camera, a decision that was driven by mass and mechanism constraints. The general concept of operations involves a 2 hour pass once every 24 hours, with passes specifically placed before all maneuvers to supply accurate navigation information to guidance and targeting. The pass lengths are limited by thermal constraints on the vehicle since the OpNav attitude generally deviates from the thermally stable tail-to-sun attitude maintained during the rest of the orbit coast

*NASA Orion Navigation Lead, Aeroscience and Flight Mechanics Division, EG6, AIAA Senior Member
†Navigation Technical Discipline Lead, Aeroscience and Flight Mechanics Division, EG6, AIAA Associate Fellow
‡Orion Navigation Hardware Subsystem Manager, Aeroscience and Flight Mechanics Division, EG2

phase. Calibration is scheduled prior to every pass due to the unknown nature of thermal effects on the lens distortion and the mounting platform deformations between the camera and star trackers. The calibration technique is described in detail by Christian, et al.[2] and simultaneously estimates the Brown–Conrady coefficients and the Star Tracker/Camera interlock angles. Accurate attitude information is provided by the star trackers during each pass. Figure 1 shows the various phases of lunar return navigation when the vehicle is in autonomous operation with lost ground communication. The midcourse maneuvers are placed to control the entry interface conditions to the desired corridor for safe landing. The general form of optical navigation on Orion is where still images of the Moon or Earth are processed to find the apparent angular diameter and centroid in the camera focal plane. This raw data is transformed into range and bearing angle measurements using planetary data and precise star tracker inertial attitude. The measurements are then sent to the main flight computer's Kalman filter to update the onboard state vector. The images are, of course, collected over an arc to converge the state and estimate velocity. The same basic technique was used by Apollo to satisfy loss-of-comm, but Apollo used manual crew sightings with a vehicle-integral sextant instead of autonomously processing optical imagery. The software development is past its Critical Design Review, and is progressing through test and certification for human rating.

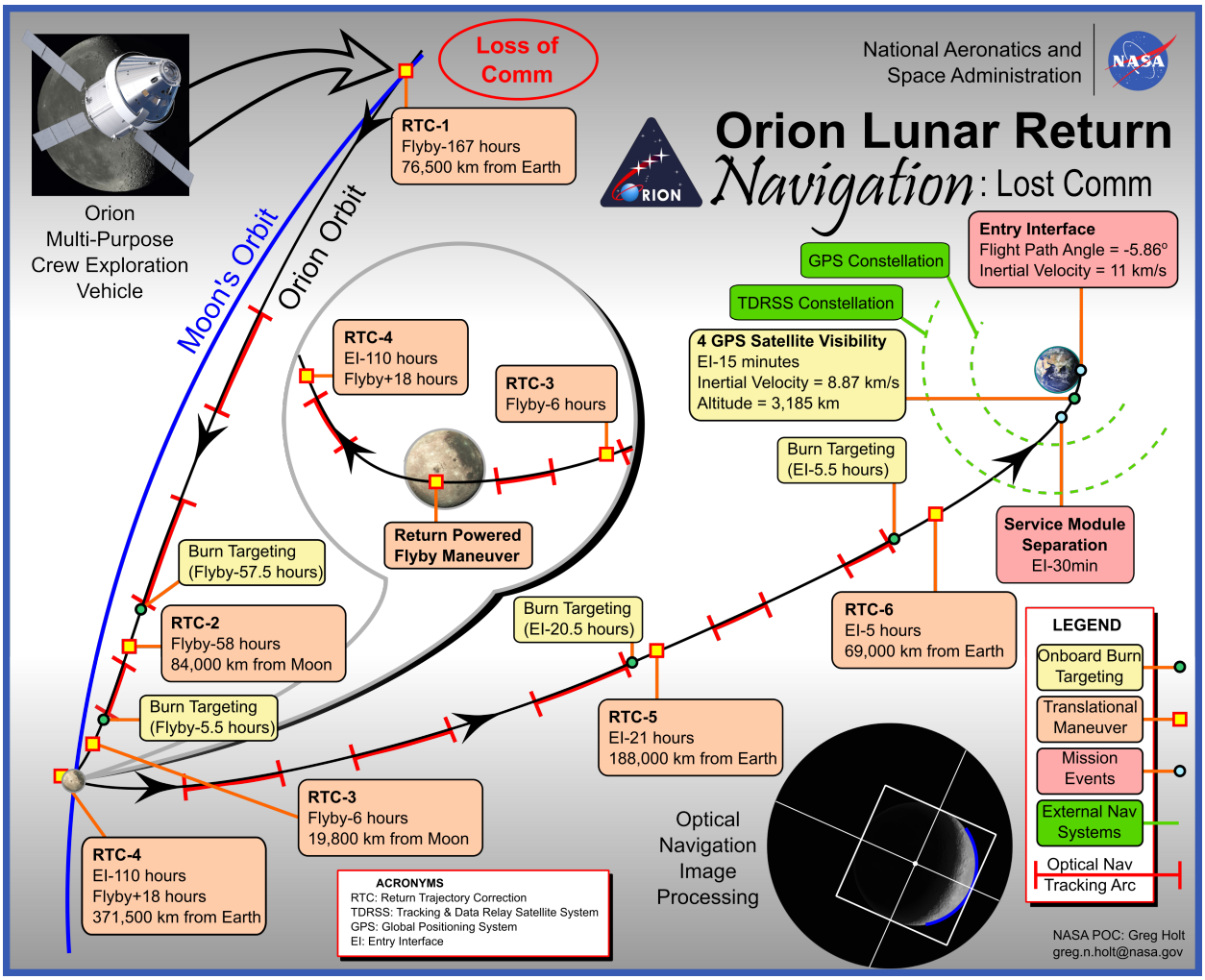

Figure 1. Orion Lunar Return Navigation Concept for Loss Of Communications

B. Navigation Architecture

The EM-1 Navigation architecture is presented in Figure 2. The navigation sensors include 3 Inertial Measurement Units (IMUs), 2 GPS Receivers, 2 Star Trackers (STs), and 1 Optical Navigation (OPNAV) camera.

The star trackers and the optical navigation camera are mounted together on an optical bench on the Crew Module Adapter (CMA).

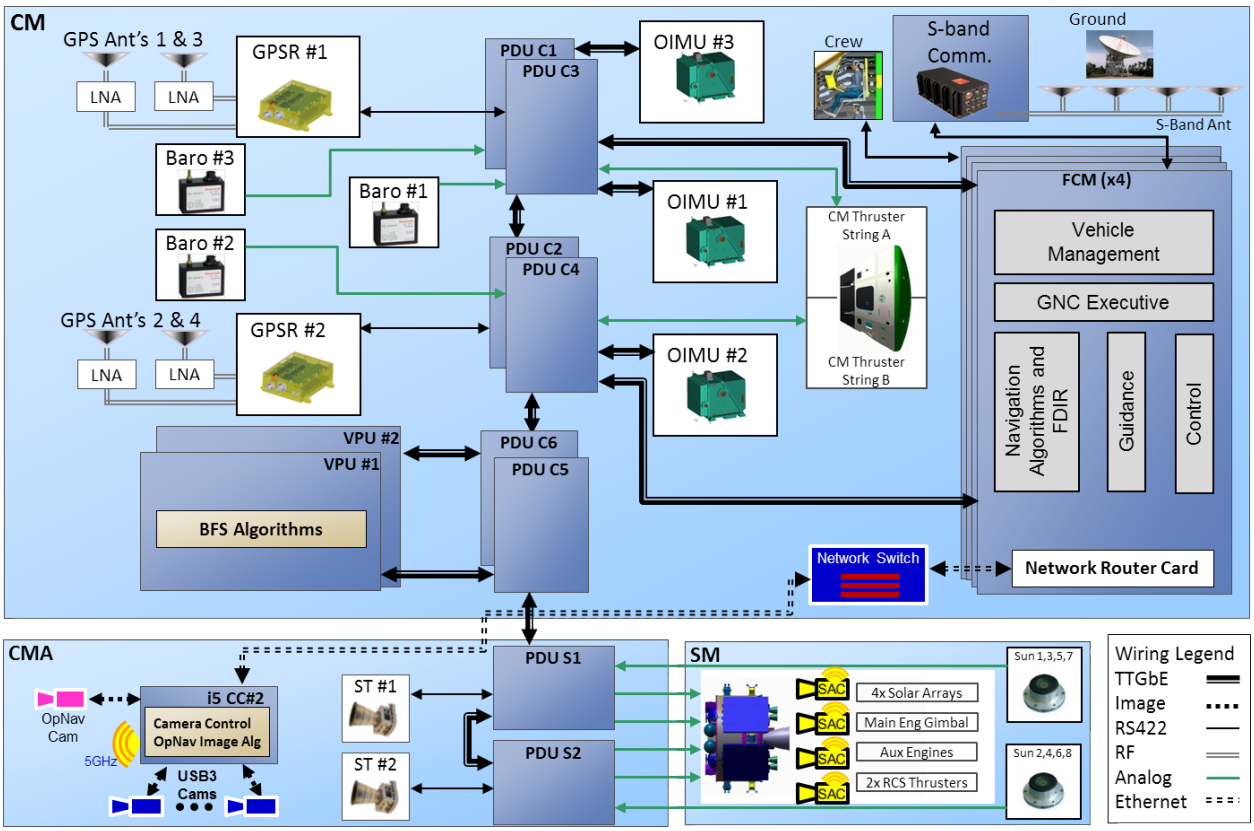

Figure 2. Orion Navigation Architecture

The navigation architecture includes a set of navigation filters configured to operate with specific sensors. There are four types of filters which are Extended Kalman Filters (EKFs): Atmospheric EKF (ATMEKF), Attitude EKF (AttEKF), Earth Orbit EKF (EOEKF), and Cislunar EKF (CLEKF).Each of these filters is modeled after a multiplicative EKF (MEKF) where the attitude error states are treated as (small) deviations from the reference attitude states and are incorporated into the attitude states in a multiplicative fashion. After each measurement cycle, the attitude state is updated and the attitude error state is zeroed out. The reference attitude state is then propagated using the gyro outputs. The Cislunar EKF, which is the filter used outside of low-earth orbit (and the GPS constellation) is an 21-state MEKF whose states are: position (3), velocity (3), attitude error (3), unmodeled acceleration (3), accelerometer biases (3), accelerometer scale factor (3), optical sensor biases (3). Since the ATTEKF is the primary filter to estimate the attitude (by processing Star Tracker measurements and gyro data), the attitude of the vehicle is not updated from the output of the CLEKF. Instead the attitude states in the CLEKF are modeled as first-order Gauss-Markov processes with process noise strength modeled to be consistent with the expected attitude error from the ATTEKF. As well the other bias states are treated as first-order Gauss-Markov processes with appropriate process noise strength and time constants. The accelerometer bias and scale factor parameters are included in this filter to account for the effects of the accelerometer errors during powered flight maneuvers. Since the accelerometers are thresholded during coasting flight, the unmodeled acceleration states are chosen in order to include the effect of non-powered accelerations imparted on the vehicle due to residual acceleration caused by attitude deadbanding, attitude maneuvers, sublimator vents, Pressure Swing Adsorption (PSA) vents, and waste-water vents. The latter two won't be a factor during EM-1 since it will be uncrewed. Finally, the presence of the Earth's atmosphere and the lunar terrain will introduce measurement biases and these effects are attempted to be captured by the optical navigation measurement states (which are modeled as slowly time varying first-order Gauss-Markov states).

The filter architecture uses a square-root-free UDU covariance factorization. The UDU factorization

was chosen for all of Orion navigation filters because of its numeric stability and computational efficiency.[3] In particular computation savings were exploited in the propagation phase by partitioning the filter states into 'states' and 'parameters'. The covariance associated with the 'states', comprising of the position and velocity, were propagated using a numerically computed state transition matrix and updated via a modified weighted Gram-Schmidt algorithm, while the covariance of the 'parameters' was propagated analytically using a rank-one Agee-Turner algorithm.[4] The measurements were updated one-at-a-time (assuming uncorrelated measurements) using a Carlson rank-one update.[5] In addition the CLEKF architecture allowed for 'considering' any of the parameter states.

II. Navigation Design and Analysis

Much of the effort in designing the Orion optical navigation system went into characterizing the measurement model and the measurement error model. The next two sub-sections are devoted to detailing these. Linear Covariance Analysis (LinCov) was used to analyze the measurement models and the measurement error models on a representative EM-1 trajectory. This is detailed in the final subsection. The non-linear least squares refinement then follows the technique of Mortari[6] as an estimation process of the planetary limb using the sigmoid function. The mathematical formulation behind the initial ellipse fit in the image processing is detailed in Christian.[7]

A. Measurements

A major focus of the efforts in the design of the CLEKF was a careful modeling of the measurement with an eye toward computational efficiency. To that end the centroid measurements were chosen to be the tangent angles rather than the 'raw' angles. In addition, the planetary diameter is chosen to be its equivalent: the range to the planet.

This manifests itself as follows:

$$y_h = \tan\alpha_h + b_h + \eta_h = x/z + b_h + \eta_h \quad (1)$$

$$y_v = \tan\alpha_v + b_v + \eta_v = y/z + b_v + \eta_v \quad (2)$$

$$\rho = \sqrt{x^2+y^2+z^2} = \left|\left|\mathbf{r}^i_{orion} - \mathbf{r}^i_P\right|\right| \quad (3)$$

The first two, y_h and y_v, are the centroid measurements and the last one is the range, which will be corrupted a bit further in this exposition by bias and noise to produce a range measurement.

If the planet is perfectly spherical, the range to the planet would be given by

$$\sin\frac{A}{2} = \frac{R_p}{\rho} \quad (4)$$

where R_p is the planetary radius and A is the angular diameter. The model assumed in this analysis is a pinhole camera model. The equivalent expression at the focal plane is

$$\tan\frac{A}{2} = \frac{n_d}{2fs} \quad (5)$$

where n_d is the number of pixels that constitute the angular diameter and s is the pixel pitch (in units of pixels per length, assuming square pixels). This is seen in Figure 3. For what follows, we define

$$\delta \triangleq \frac{n_d}{fs} \quad (6)$$

where δ is a non-dimensional quantity and is the "raw" measurement of the planetary diameter. Consistent with the centroid measurements. Given that the measurements are corrupted with noise, the actual planetary diameter measurement is

$$\tilde{\delta} = \delta + b_d + \eta_d = 2\tan\frac{A}{2} + b_d + \eta_d \quad (7)$$

Given that Eq. (5) can be expressed as

$$\tan\frac{A}{2} = \frac{\delta}{2} \quad (8)$$

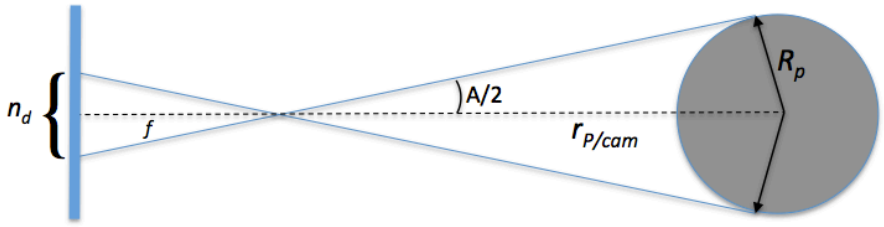

Figure 3. Angular Diameter Measurement

using elementary trigonometry, the above equation (Eq. (8)) can be written as

$$\sin\frac{A}{2} = \frac{\delta}{\sqrt{\delta^2+4}} \tag{9}$$

Eq. (4) and Eq. (9) are equated to solve for δ yielding

$$\delta = \frac{2R_p}{\sqrt{\rho^2 - R_p^2}} \tag{10}$$

or equivalently ρ can be written in terms of δ as

$$\rho = R_p\sqrt{1+\left(\frac{2}{\delta}\right)^2} \tag{11}$$

and acknowledging the fact that the measurement is corrupted with noise and bias, we get

$$y_\rho = R_p\sqrt{1+\left(\frac{2}{\delta+b_d+\eta_d}\right)^2} \tag{12}$$

B. The Measurement Error Calculations

In LinCov we model the pixel centroid measurements as

$$u = u_p - fs\tan\alpha_h = u_p - fs\,y_h \tag{13}$$
$$v = u_p - fs\tan\alpha_v = v_p - fs\,y_v \tag{14}$$

so that

$$du = -(fs)dy_h \tag{15}$$
$$du = -(fs)dy_h \tag{16}$$

With this in hand,

$$\sigma_u = (fs)\,\sigma_{y_h} \tag{17}$$
$$\sigma_v = (fs)\,\sigma_{y_v} \tag{18}$$

and

$$\sigma_{y_h} = \frac{1}{fs}\,\sigma_u \tag{19}$$
$$\sigma_{y_v} = \frac{1}{fs}\,\sigma_v \tag{20}$$

We have been assuming in LinCov that the pixel pitch is 4.8×10^{-6} m/pixel and the focal length is 35.1 mm so that

$$\frac{1}{fs} = 1.3675 \times 10^{-4} \,\text{pixels}^{-1} \tag{21}$$

which is equivalent to 28.2 arc-seconds per pixel ($= 1.3675 \times 10^{-4} \cdot 3600 \cdot 180/\pi$)

Given that

$$\delta = \frac{n_d}{fs} \tag{22}$$

the error in these are found to be

$$d\delta = \frac{1}{fs} dn_d \tag{23}$$

and

$$d\rho = -\frac{\rho^2 - R_p^2}{\rho} \frac{d\delta}{\delta} = -\frac{\rho^2 - R_p^2}{\rho} \frac{dn_d}{n_d} \tag{24}$$

The standard deviation can be approximated as

$$\sigma_\rho = \frac{\rho^2 - R_p^2}{\rho} \frac{1}{n_d} \sigma_{n_d} \tag{25}$$

which for $\rho >> R_p$ becomes

$$\sigma_\rho = \frac{\rho}{n_d} \sigma_{n_d} \tag{26}$$

This is the error for a 'smooth' Moon. Terrain effects add additional error which diminishes as the range increases as

$$\sigma_\rho = \sqrt{\sigma_{r_{\text{smooth}}}^2 + \left(\sigma_{r_{\text{terrain}}}(\rho)\right)^2} \tag{27}$$

The measurement errors are described in Christian.[8] The errors associated with lunar tracking are greatly influenced by the lunar terrain. In particular, the errors are tied to the portion of the Moon being observed. Since there are a limited number of lunar images available which have usable time-tags, attitude of the camera and truth data available, computer generated images using Engineering DOUG Graphics for Exploration (EDGE) were used. EDGE simulates the lunar terrain using the latest Lunar Reconnaissance Orbiter (LRO) topography and imagery and is particularly useful because the lighting and distance can be varied. EDGE was also used to generate Earth imagery with improved atmospheric models. A representative EM-1 trajectory was used to generate EDGE (Earth and Moon) images to vary the lighting conditions at different points in the trajectory as well as to investigate the effects of looking at different portions of the Moon. This was then used to obtain the following Moon noise error models:

$$\sigma_r = \sqrt{(0.12\,\text{pix})^2 + \left(\frac{7291.7\,\text{pix})(6562\,\text{ft})}{\rho}\right)^2} \tag{28}$$

where ρ is the distance in feet and σ_r is the resulting radius error in pixels. The centroid angles are dependent on the illumination direction. Hence, centroid errors parallel and perpendicular to the Moon-Sun direction (α and β, respectively) were developed, once again using EDGE imagery, and are as follows:

$$\sigma_\alpha = \sqrt{(0.15\,\text{pix})^2 + \left(\frac{7291.7\,\text{pix})(6562\,\text{ft})}{\rho}\right)^2} \tag{29}$$

$$\sigma_\beta = \sqrt{(0.06\,\text{pix})^2 + \left(\frac{7291.7\,\text{pix})(6562\,\text{ft})}{2\rho}\right)^2} \tag{30}$$

The factor 6562 ft has to do with the expected lunar terrain variation across the lunar surface of 2 km.

The bias for Moon imagery was generated by looking only at one side of the Moon and is:

$$b_\alpha = (0.383\,\text{pix}) - \frac{3.470 \times 10^8\,\text{pix} - \text{ft}}{\rho} \tag{31}$$

$$b_\beta = 0 \tag{32}$$

$$b_r = (-0.236\,\text{pix}) - \frac{1.964 \times 10^8\,\text{pix} - \text{ft}}{\rho} \tag{33}$$

For Earth imagery the noise in analyzing EDGE imagery was found to be

$$\sigma_\alpha \approx 0.065\,\text{pix} \tag{34}$$

$$\sigma_\beta \approx 0.025\,\text{pix} \tag{35}$$

$$\sigma_r \approx 0.058\,\text{pix} \tag{36}$$

$$\tag{37}$$

with a bias on the radius measurement to be

$$b_r = (-0.263\,\text{pix}) - \frac{1.901 \times 10^8\,\text{pix} - \text{ft}}{\rho} \tag{38}$$

Obviously this is a function of the expected atmosphere 'bias' (in the case above the atmospher bias was taken to be 35 km) and a the sensitivity to this has been performed.

C. LinCov Results

The Linear Covariance results are (obviously) highly dependent on the measurement and measurement error models used. To that end, in keeping with the design of the flight software, the environment measurement model was for the Moon was taken as described above. For Earth-measurement passes, the noise models were taken to be the same as the Moon because they were more conservative than the EDGE-generated Earth imagery provided.

The filter (FSW) measurement error models were taken to be a constant and measurement passes very close to the Moon were not performed because of the large bias errors (due to lunar terrain) and the FOV of the camera. Analysis performed to date shows a delivery that satisfies an allowable entry corridor as shown in Figure 4.

III. Hardware and Software Tests

One of the main difficulties in testing and verification of the OpNav system is the lack of on-orbit imagery with high-fidelity metadata as a truth source. A combination of hardware characterization, live-sky testing, and synthetic imagery were therefore used to test the system.

A. Camera Calibration and Focus

The Orion EM-1 flight camera was calibrated at the Johnson (JSC) electro-optics lab as seen in Figure 6. The camera requires extrinsic calibration prior to the flight for the default load of the lens distortion parameters. Additionally, we needed to permanently stake the focal length of the lens to just under infinity. This keeps the focus from shifting during ascent vibration. Slightly focusing under infinity allows spread of the energy across multiple pixels for sub-pixel resolution. A flat field and modulation transfer function evaluation were also accomplished as part of the exercise as well.

All camera lenses add radial distortion to an image and sensor misalignment will add tangential distortion. Without accounting for these distortions, optical navigation measurements will yield inaccurate results. These distortions are mapped and eliminated by warping the image in the opposite direction of the distortion before using them for centroiding and limb finding. This process is called calibration.

The calibration was carried out using a two-axis gimbal and large collimator to account for camera distortions due to lenses and sensor misalignment. This is completed by fastening the camera to a rotation

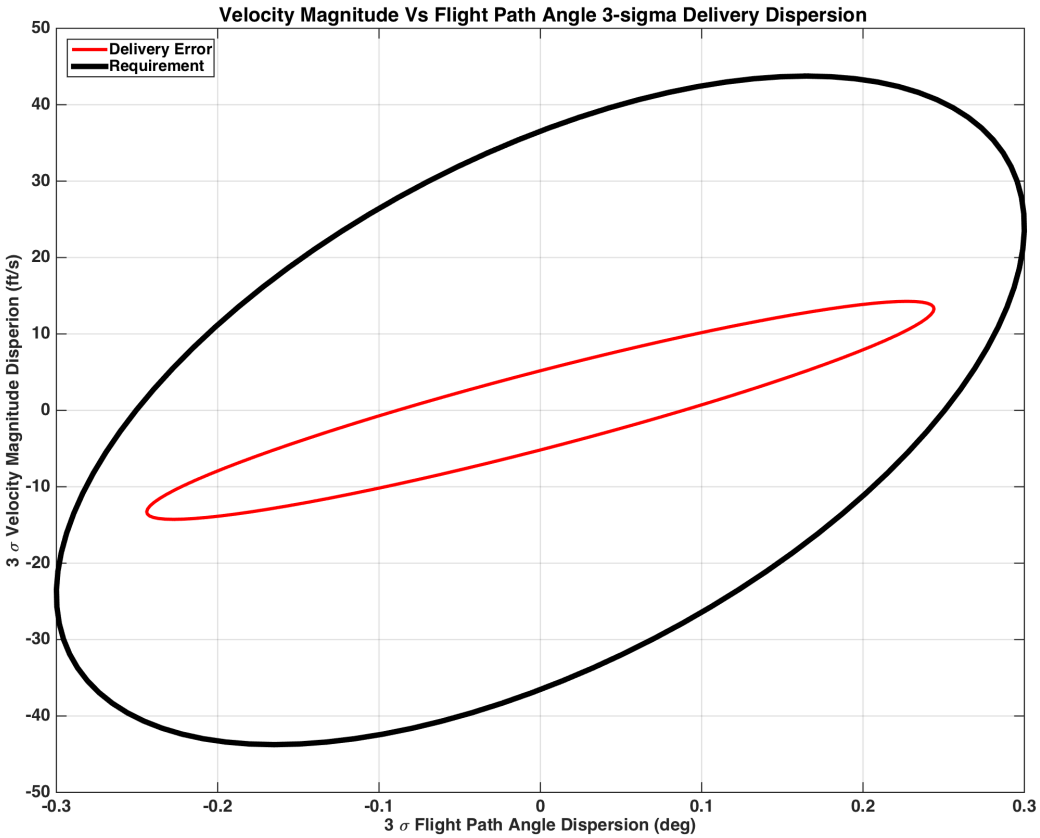

Figure 4. Orion Entry Interface Delivery Dispersions vs. Corridor Requirement

stage on the gimbal and panning along the horizontal field of view of 19.5 deg and a vertical field of view of 15.6 deg in increments of 2 deg. The camera captures a total of 99 images which are then combined to make a single composite star grid. The camera exposure was set within 1-5 ms range to avoid saturation of pixels from the collimated light source used.

This star map is then used to create a distortion contour plot as show in Figure 5. A pinhole camera model was used to generate these plots and associated software, characterized by the error shown in equation 39.

$$\begin{aligned} x' &= -tan(\alpha)\frac{fl}{dx} \\ y' &= -tan(\beta)\frac{fl}{dy} \\ Error &= \sqrt{(x-x')^2+(y-y')^2} \end{aligned} \tag{39}$$

where α, β are the skew angles, fl is the focal length of 43.3mm, and dx, dy are the vertical and horizontal pixel pitch of 0.018 mm/pixel. To permanently stake the focal length of the camera a 500 mm focal length refractive collimator was used. This device has an objective diameter of 50mm with a 15-micron pinhole reticle light source to simulate a single star. The camera and equipment or mounted on a steady base optical table on a steady floor and a computer is used to control the camera. Using a calibrated torque wrench the focus is adjusted using the lens focus lock screw while using the software and collimator to locate the star within the center of the camera area and focus it to infinity and no pixel is saturated. This process takes several iterations and a final slight defocus is accomplished before tightening and staking with a staking compound to hold the lens in place permanently.

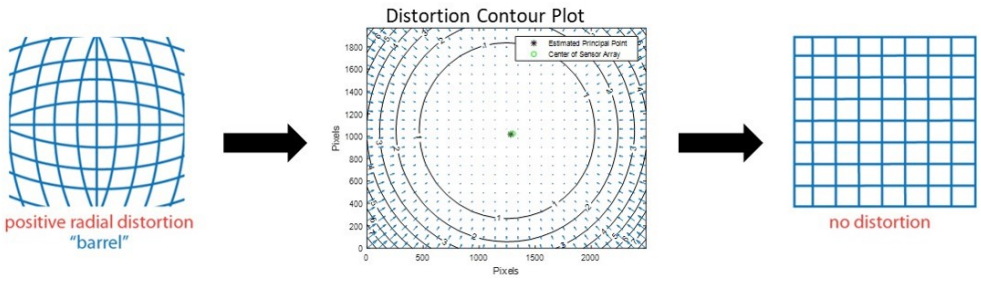

Figure 5. Pinhole Camera Distortion Model

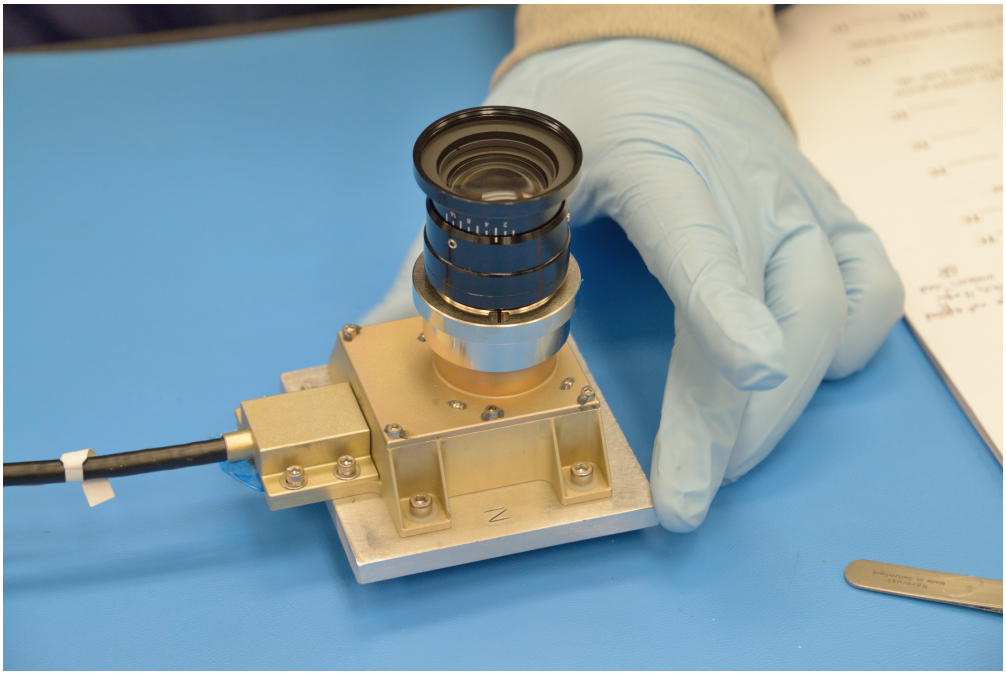

Figure 6. Orion EM-1 Optical Navigation Camera Calibration (*Photo courtesy NASA/Mike Ruiz*)

B. Live Sky Test

Two Engineering Design Unit (EDU) cameras and an EDU star tracker were used for a live-sky test in Denver, as shown in Figure 7. The star tracker was used as a truth attitude reference in taking simulated calibrations and measurements from the EDU cameras. Both starfield and moon images were taken for the purposes of calibration and taking measurements, respectively. The test provides valuable live-sky imagery, since synthetic imagery always has inherent limitations when modeling real-world effects. As mentioned before, in-space imagery with high-fidelity truth metadata is rare so these live-sky tests provide one of the closest real-world analogs to operational use.

The test was performed on a clear night at a temperature between 0 and 30 degrees C with a relative humidity of less than 65%. The Star tracker and Optical Cameras were mounted on a rigid 8 inch (203.2 mm) by 10 inch (254 mm) anodized aluminum plate that was oriented and aligned using a standard magnetic compass and compensated for local magnetic declination. One of the cameras was mounted on an angled plate that could be adjusted in order to track the moon in its field of view while the Star Tracker and other optical camera stayed static. Several sets of images along with the metadata needed from the Star Tracker were collected to test the optical navigation algorithms and help model real effects for simulations testing and certification.

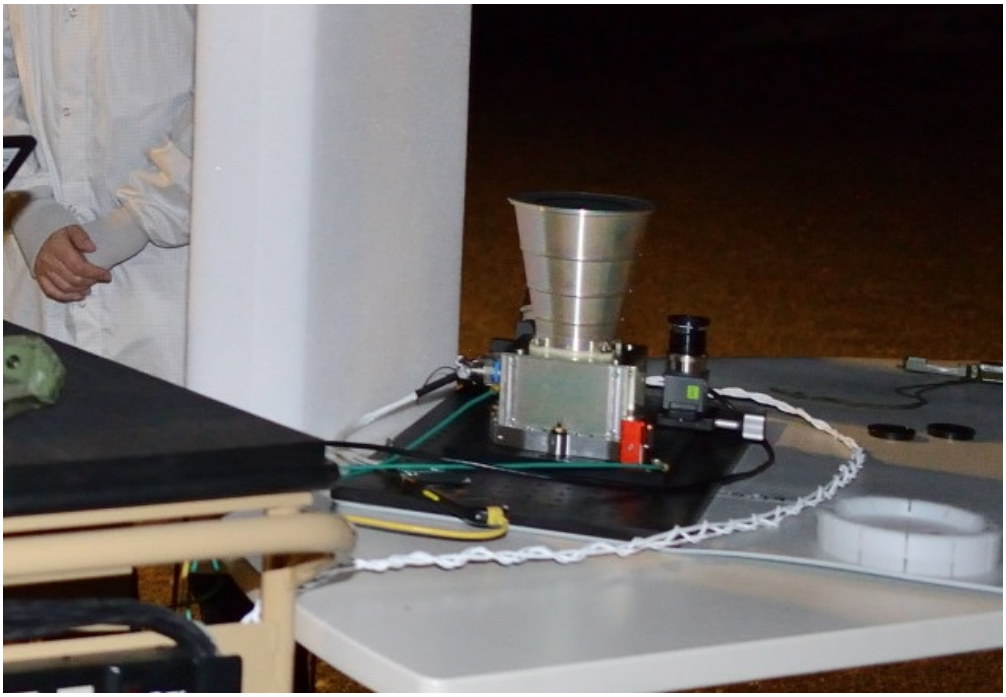

Figure 7. The EDU camera and star tracker rig are set up for a live-sky test in Denver (*Photo courtesy NASA/Steve Lockhart*)

C. Hardware-in-the-Loop Lab Test

In support of systems-level verification, a hardware-in-the-loop test rig was developed in the Johnson Space Center Electro-Optics Lab to exercise the OpNav system prior to integrated testing on the Orion vehicle. Figure 8 shows the rig, which the test team has dubbed OCILOT (Orion Camera In the Loop Optical Testbed). The rig consists of an EDU opnav camera, a collimating lens, and a dense pixel display all mounted on an optical bench and micro-alignment brackets. The formal hardware-in-the-loop verification rig uses an 8K display and an additional field flattening lens. The hardware test allows for integrated test of all the data flow, hardware connections, and real avionics.

D. Software Verification Testing

The software is primarily verified with synthetic imagery for which definitive truth data is available. The simulated camera field of view is shown in Figure 9. The images are generated using EDGE, which was specifically upgraded to include high-fidelity lunar terrain, Earth atmospheric scattering, and stellar aberration which effects measurements and calibration respectively. The nominal conceptual flight profile is used to verify performance metrics. Several hundred off-nominal images are also used to analyze robustness and fault detection in the software. These include effects such as stray light, excess radiation damage, specular reflections, etc. An example of the verification images is shown in Figure 10, where images of the Earth and Moon are tested. Of note is the stressing case in Figure D, where the crescent is quite thin. These tests also help verify the tuning parameters chosen for the algorithm such as earth atmosphere bias, minimum pixel intensity, and star detection thresholds.

Acknowledgments

The authors would like to thank the outstanding team at Johnson Space Center for their contributions to getting us where we are today, with particular gratitude to Lorraine Prokop and Steven Lockhart. Additionally, the support of contractor partners at Lockheed Martin Space Systems was very appreciated. Finally, we would also like to acknowledge the assistance of professors John Christian, Daneila Mortari, and Renato Zanetti in algorithm research.

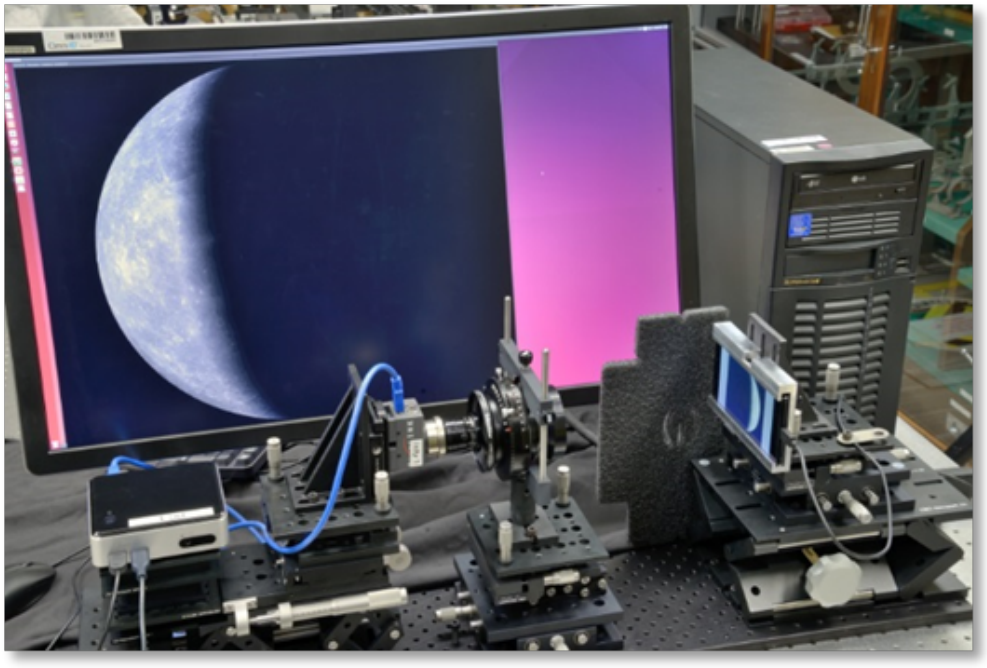

Figure 8. Orion Camera In the Loop Optical Testbed (*Photo courtesy NASA/Steve Lockhart*)

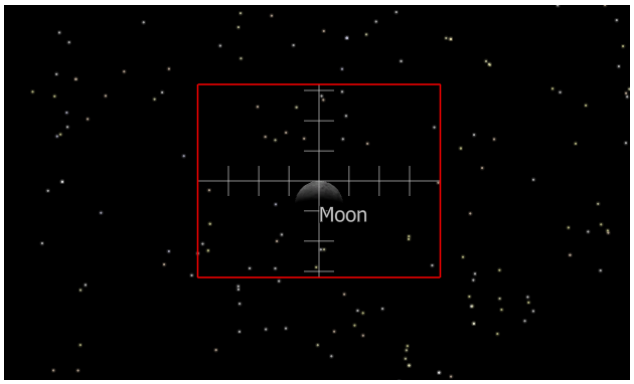

Figure 9. Simulated opnav camera field of view capturing moon image

(a) Earth Image (b) Moon Image (c) Stressing Moon Image

Figure 10. Synthetic Imagery Used for verification

References

[1]Battin, Richard H., "An Introduction to the Mathematics and Methods of Astrodynamics", AIAA Education Series, Revised Edition, 1999.

[2]Christian, John A., Benhacine, L., and Hikes, J. et al., "Geometric Calibration of the Orion Optical Navigation Camera Using Star Field Images, The Journal of the Astronautical Sciences, Vol. 63, No. 4, Dec. 2016.

[3]Bierman, G. J., *Factorization Methods for Discrete Sequential Estimation*, New York: Dover Publications, 2006.

[4]Agee, W.S. and Turner, R.H., "Triangular Decomposition of a Positive Definite Matrix Plus a Symmetric Dyad with Application to Kalman Filtering, White Sands Missile Range Tech. Rep. No. 38, 1972.

[5]Carlson, N.A., "Fast Triangular Factorization of the Square Root Filter", AIAA Journal, Vol. 11, No. 9, September 1973.

[6]Mortari, Daniele, C. N. D'Souza, and R. Zanetti, "Image Processing of Illuminated Ellipsoid", Journal of Spacecraft and Rockets, Vol. 53, No. 3, May-June 2016.

[7]Christian, John A., "Optical Navigation Using Planet's Centroid and Apparent Diameter in Image", AIAA Journal of Guidance, Control, and Dynamics, Vol. 38, No. 2, Feb 2015.

[8]Christian, John A., "Error Model for OPNAV Centroid and Radius Measurements", Technical Memorandum, RPI/SEAL-17-001, Rensselaer Polytechnic Institute, October 2017.